POLITECNICO DI TORINO
Repository ISTITUZIONALE

Compact Extended Scan Range Antenna Array based on Rotman Lens

(Article begins on next page)

22 September 2024

Compact Extended Scan Range Antenna Array based on Rotman Lens

Enrico Tolin, Oliver Litschke, Simona Bruni, and Francesca Vipiana, *Senior Member, IEEE*

Abstract— The present paper proposes an innovative method for extending the scan range of phased arrays based on Rotman lens by a factor two. The main objective is to take advantage of the performance of the Rotman lens as beamforming network, resolving its intrinsic increase of phase error and coupling losses when wide scan angles are required. The proposed concept aims to overcome these limitations, by introducing the combination of two specific operations called "Complete Beam Shifting" and "Beam Mirroring". The described technique is applied to a 24 GHz scanning array antenna system, designed and manufactured by taking into consideration fabrication and related cost issues. Finally, the proposed concept has been validated through measurements.

Index Terms—Beam steering, linear antenna arrays, microstrip antenna arrays, phased arrays, beamforming networks, Rotman lens.

I. Introduction

PHASED array antennas represent a key component for many applications, ranging from satellite communication to surveillance systems. Their wide spreading application leads to a raise in technology development, which increased the requirement of an array antenna system with high performance, low cost and easy integration. Two of the main and most important applications of scanning arrays are radar and communication systems.

Radar technology is growing exponentially in recent years, with an increasing trend due to the technical advancement in customary markets like automotive, space or military, and the exploitation of these devices in sensors for industrial, automation and surveillance applications. A notable example of its application is the Advanced Driver Assistant System (ADAS), which represents one of the key elements that support the autonomous driving research and development, following the goal of a Highly Automated Driving (HAD) by 2020, for highway driving scenarios, and the final introduction of fully automated driving after the year 2025 [1]. Moreover, also communication systems have encountered an exceptional technological development in recent years, due to the increasing demand of coverage and high data rate.

In order to meet these requirements, communication systems are evolving through beam switching or beam steering millimeter wave solutions in the V- and W- bands (50 – 110 GHz). In the highlighted contexts, significant interest has gained the Rotman lens as Beam Forming Network (BFN). The trifocal Rotman lens was first proposed by Rotman and Turner in the 1960s [2], and since then many studies have developed new approaches for the definition of the lens geometry and its physical design (see e.g. [3]-[8]). In particular, this kind of BFN is very attractive because it is a True Time Delay (TTD) device (thus intrinsically broadband), it is relatively simple to design, it supports multiple beams and, if proper designed, it exhibits low losses and an accurate progressive phase distribution over all its outputs. Moreover, its manufacturing is very convenient for most applications, due to its monolithic planar structure, which is light weight, easy to produce and low cost.

Many researches have been carried for improving the performance of Rotman lens, by calculating a more efficient lens geometry [9]-[12], or by optimizing its construction [13]-[14]. Furthermore, state-of-the-art technologies have been applied to the Rotman lens design for enhancing its performance, by exploiting Substrate Integrated Waveguide (SIW) [15]-[16], Low Temperature Cofired Ceramic (LTCC) [18], or either introducing synthesized dielectric substrates [20], multilayer design [20] or Ridge Band Gaps (RBG) [21]. Despite the good performance level and the positive manufacturing considerations, the design of the Rotman lens became complicated when wide scan angles are required. The reason for the high inaccuracies of this kind of BFN, concerning the phase distribution and beam level in relation to wide scan angle, is given by the intrinsic geometry of the lens, which assumes excessive and inefficient shapes. Nevertheless, few achievements have been published for improving this aspect of the Rotman lens. The most representative is found in [22], where piezoelectric transducer (PET) controlled phase shifters were used for increasing the steering angle by 8°, for a total scanning range of ±38°. In a similar way, in [23], liquid crystals (LC) phase shifters were used in combination with the Rotman lens to increase the scanning range by ±7.5°.

This paper is focused on the development of a compact, inexpensive and high-performance method for broadening the overall scanning range of a BFN by a factor two. The method is based on the application of a specific phase management unit, realized with an innovative and efficient reconfigurable phase shifter, in cascade with the BFN. The proposed method, with respect to the previous researches, considerably broaden the Field of View (FOV) while using standard PIN diodes and regular Printed Circuit Board (PCB) technology, in contrast

with the PET approach that suffer from tribology problems [22], and the use of LC, whose manufacturing is much more complex due to its fluid nature [23]. Moreover, the use of PIN diodes allows to use low voltages, and then to be compatible with digital signals instead of high voltages (up to 60V in the case of PET), while having an accurate phase shifting response and comparable losses. The proposed method for broadening the scan range is first applied to a general linear array, and, then, we investigate its combination with the Rotman lens in order to realize a system that combines the features of the Rotman lens with a wide scanning angle. The designed Rotman lens BFN, fabricated in PCB technology, is meant to be used in a radar system, for application based on the 24 GHz ISM band. The performance of the extended scan range BFN based on Rotman lens are evaluated with numerical methods and finally validated through measurements.

In addition, a novel concept for feeding the lens has been implemented for the first time. This innovative feeding is based on a two-way connection of beam ports made by sequential arrangement of Wilkinson combiners [24], in order to provide a more efficient illumination of the array ports and then increase the overall performance of the system. The present work validates the preliminary numerical results shown in [25], and replaces the design of the phase management unit of [26]-[27], with a much more compact and high-performance solution.

II. EXTENDED SCAN RANGE METHOD

Two operations concerning the phase are applied at the output of the considered BFN. These operations are named as "Complete Beam Shifting" (CBS) and "Beam Mirroring" (BM). The generic array factor $AF(\theta,\varphi)$ of a N-elements linear array is considered,

$$AF(\theta) = \sum_{n=1}^{N} I_n e^{j(n-1)(kd\sin\theta+\Phi)} \underbrace{e^{j\alpha_n}}_{CBS} \underbrace{e^{j\beta_n}}_{BM}, \quad (1)$$

referring to the case of array elements arranged along the x axis, with uniform spacing d, uniform phase gradient Φ between adjacent array elements, and antenna radiation pattern in the xz plane. In (1), j is the imaginary unit, I_n is the amplitude of n-th element excitation, and k is the wavenumber. The two phase factors $e^{j\alpha_n}$ and $e^{j\beta}$ are the phase contributions of the CBS and the BM respectively; hence, the extended scanning range method involves two operations superimposed to the BFN phase distribution. In particular, the CBS is a general approach to move all the radiated beams in such a way that just one portion of the scan range is covered (either positive or negative). In other words, when the CBS is applied to an initial phased array scanning in the range $\pm\theta_{max}$, the outcoming scan is then modified to cover the range from 0 to $2\theta_{max}$. This process is made possible by the application of a progressive phase shift superimposed to the canonical phase distribution produced by the BFN. The additional phase term, $e^{j\alpha_n}$ in (1), that defines the CBS, can be written as:

$$\alpha_n = n \cdot k \cdot d \cdot \sin(\theta_{max}), \quad (2)$$

with $n = 1, 2, ..., N$ is the n-th array element.

Similar considerations discussed for the CBS can be applied to the BM. This operation produces a reversal of the sign of the radiated beam pointing angle by the application of proper phase distribution at the array input. The phase term $e^{j\beta_n}$ in (1), that accounts for the BM, can be expressed as

$$\beta_n = -(2n-1) \cdot k \cdot d \cdot \sin(\theta_{max}), \quad (3)$$

where $n = 1, 2, ..., N$. It can be easily verified that the application of the term $e^{j\beta_n}$ to the considered n-th radiated beam introduces in the xz plane a shift in the pointing angle of $2\theta_{max}$: e.g. the beam previously pointing to $2\theta_{max}$, due to the application of the CBS, is now pointing to $\theta = 0$.

Therefore, the combination of the CBS and BM applied to the original BFN phase distribution allows to provide a doubling of the initial scanning range. First, all the beams are repositioned in the positive portion of the scanning range by applying the CBS, and consequently they are shifted completely toward the negative side by using the BM. However, the BM operation must be applied only when negative angles are needed for scanning. In other words, the phase management unit (PMU) must be *reconfigurable* for adapting the system to scan either positive or negative angles.

Analyzing the proposed progressive phase shifting used to extend the array scanning range, a convenient case can be recognized when $\theta_{max} = 30°$ and the distance d between the antenna array elements is set as $\lambda/2$, where λ is the operative wavelength. If $\theta_{max} = 30°$, in (2) the phase term simplifies to $\alpha_n = n \cdot \frac{\pi}{2}$, and hence a 90° based progressive phase shift, superimposed to the BFN initial phase distribution, is needed to redefine an initial scan range of $\pm30°$ to the range $0° - 60°$. On the other hand, in this case, (3) is also based on multiples of 90°. It can be verified that the sum of the phase contributions of BM and CBS corresponds to a -90° progressive phase shifting, i.e. $\alpha_n + \beta_n = (1-n) \cdot \frac{\pi}{2}$.
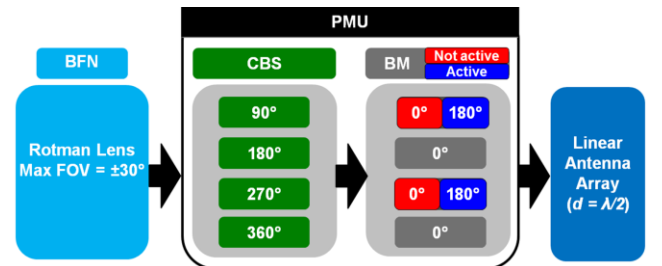
Fig. 1. Detail of the basic phase distribution given by the CBS and BM in the case of an initial Rotman lens scanning between ±30° and a linear array with spacing $d=\lambda/2$.

Fig. 1 illustrates the described concept, considering a basic block of 4 multiples of 90° for the CBS (the same is repeated for all the successive ports). Therefore, it can be noticed that there is no need to change the phase shifting at every line by the application of the BM, because we can take advantage of the half wavelength multiples. By this simple assumption, a negative version of the odd multiples of 90° can be generated

by the phase inversion at odd index of array input ports. Hence the phase management unit can be realized with a microwave circuit that combines both the CBS and BM operations through a suitable 1-bit control.

III. WIDE RANGE SCANNING ARRAY DESIGN

The concept described in Sect. II is here exploited for the design of a scanning array system using the Rotman lens as beamforming network, shown in Fig. 2 . The goal of this work is to develop a wide scanning range 24 GHz radar (the 24 GHz ISM operational bandwidth is $24 - 24.25$ GHz) suitable to be integrated in an automotive system. Due to the complexity of the system, the full wave software EMPIRE XPU [28] has been used for modeling and optimizing all the parts shown in Fig. 2.

Moreover, a multilayer design has been considered for placing the two larger components, which are the linear antenna array and the Rotman lens, on top and bottom side respectively. This choice introduces the degree of freedom of selecting different substrates for both antenna and feeding, as is clarified from the bottom inset of Fig. 2, thus extending the solutions that can be adopted for the antenna array design. Therefore, a compact PMU, able to produce the necessary phase distribution for the application of the extended scan range method, is required together with the introduction of a suitable layer-to-layer transition for accomplishing the connection between the Rotman lens and the linear array.
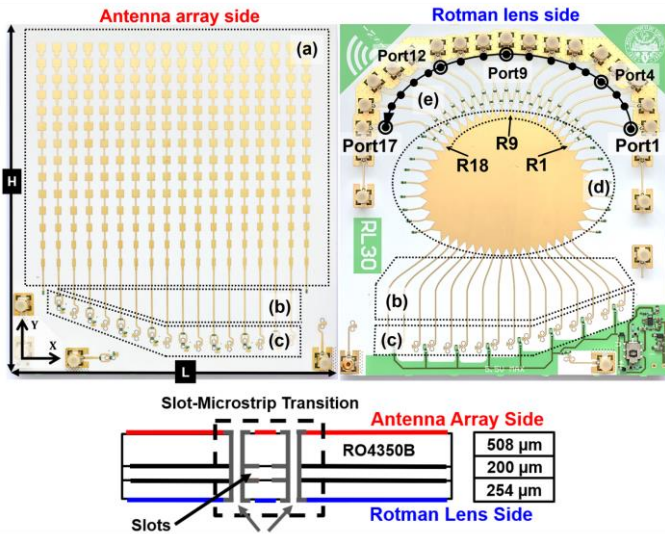

Fig. 2.   Wide Range Scanning array: "Antenna array side", "Rotman lens side" and PCB stack-up. Highlighted parts: *(a)* linear antenna array, *(b)* CBS realized through microstrip lines, *(c)* BM realized with reconfigurable phase shifters and microstrip-slot transitions, *(d)* Rotman lens and *(e)* double feeding network. System and Rotman lens input ports names are inserted for reference.

A. Rotman Lens

According to the considerations described in Sect. II, a 24 GHz tri-focal Rotman lens capable to provide steering angles between $\pm 30°$ has been designed [3], [7]. Moreover, in order to have a pattern suitable for radar applications (i.e. a good coverage of the azimuthal plane and good angular accuracy), and by considering also tradeoffs with design complexity, a

Rotman lens with 18 beam ports and 16 array ports has been developed. Finally, 8 dummy ports have been placed on both sides, for avoiding any unwanted reflection inside the lens cavity. The designed Rotman lens, shown in the Fig. 2(d) enclosure, is implemented on a 254 µm thick Roger RO4350B substrate (as indicated in the bottom inset of Fig. 2), characterized by a relative permittivity of 3.66 and loss tangent of 0.004 at 24 GHz.

As all lenses, also the Rotman lens needs to be properly illuminated for ensuring good performance. Here, a novel method for improving the Rotman lens feeding is exploited [24]. With the proposed method the Rotman lens is fed by using a series of Wilkinson dividers for simultaneously excite two consecutive Rotman lens inputs. In Fig. 2(e) enclosure, the introduced double feeding of the Rotman lens is highlighted. The designators for ports of the complete system are identified with suffix *Port-,* when double feeding is used, and Rotman lens inputs are labelled with suffix *R-*. Indeed, in analogy with the array theory, the simultaneous excitation of two elements (i.e. beam ports tapers can be considered as horns that feed the Rotman lens) leads to a more directive field distribution that illuminates the array contour on the opposite side. Fig. 3 shows the comparison between the case when just one feeding is used to excite the lens (a), and when the double feeding concept is applied (b). It is clear that a more concentrated field distribution is present in the second case. The more directive illumination decreases the losses due to the leakage on the sides, where dummy ports are foreseen, as shown in Fig. 3(b).
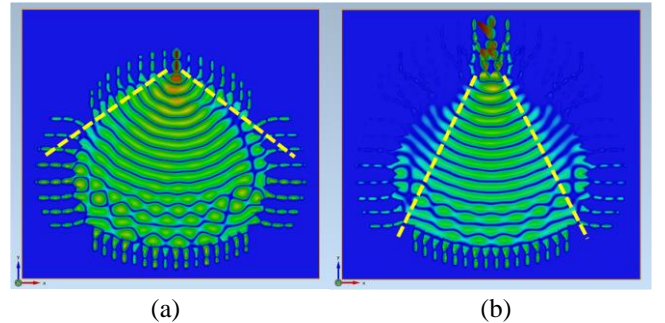

(a)   (b)

Fig. 3.   Simulated wave propagation in a Rotman lens in the case of *(a)*: standard feeding approach and *(b)* double feeding concept; the dashed lines enclose the area where most of the energy is present.

Beside this qualitative analysis, the improved Rotman lens efficiency can be directly estimated by comparing the power distribution with and without the employment of the double feeding concept. In order to evaluate the efficiency, the total insertion loss is calculated by considering the sum of the power at all beam ports. The illumination loss is defined as the port-to-port integration of power coupled with the dummy ports (spillover losses) and with the unused inputs (coupling losses). Since the efficiency of the lens is strongly dependent on the position of the excited input, different ports have been assessed: ports *R1*, *R4* and *R9* (associated with the Rotman lens without double feeding), and *Port1*, *Port4* and *Port9* (related to the design including the double feeding). In this way, the worst case concerning spillover losses (i.e. most external input), the best case of illumination (i.e. central port), and an intermediate case

are analyzed. The simulated parameters of the listed ports have been reported in Fig. 4.
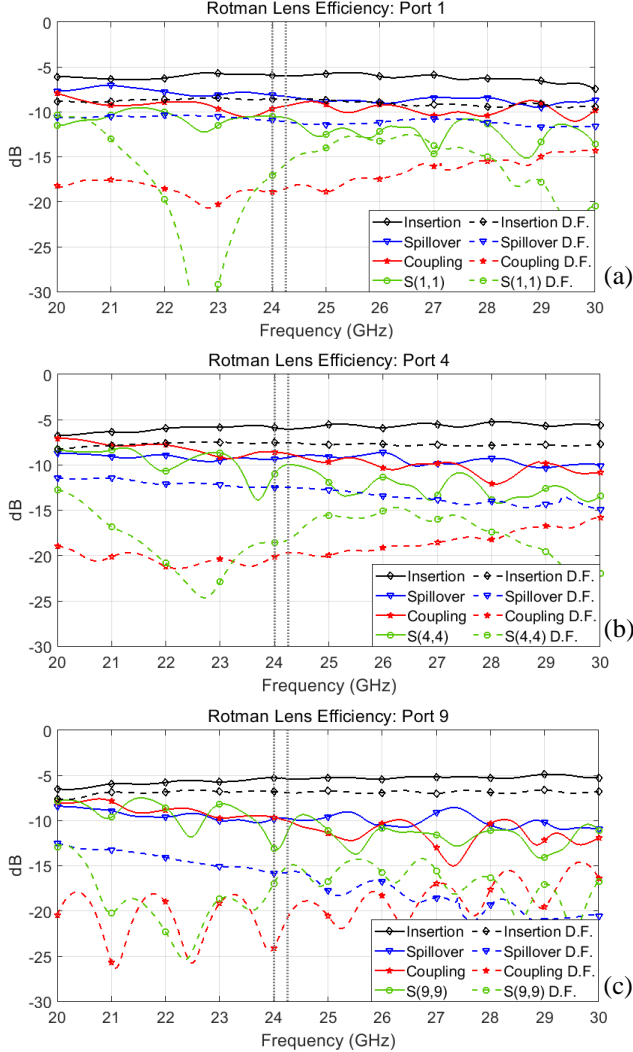

Fig. 4. Simulated Rotman efficiency in the cases with (dashed lines) and without (solid lines) the Double Feeding (D.F.); *(a) Port1* and *R1*, *(b) Port4* and *R4 and (c) Port9* and *R9*; 24 GHz ISM band is highlighted for reference.

By applying the double feeding, also in the worst case (*Port1*) shown in Fig. 4(a), the spillover losses are reduced due to the more directive propagation inside the lens cavity, as graphically demonstrated in Fig. 3(b). The coupling losses are also strongly reduced (of around 10 dB in the 24 GHz ISM band) by inserting the network composed by Wilkinson dividers, due to the further increasing of decoupling between adjacent ports. Moreover, the reflection coefficients of the Rotman lens are improved by the double feeding network, from 7 dB as displayed in Fig. 4(b) to 3 dB in the case of Fig. 4(c), in the 24 GHz ISM band.

By considering the Rotman lens without double feeding, the insertion loss is found to be between -6 dB and -5.3 dB in the band of interest, mostly due to illumination and conductive losses (conductivity of the surface finishing given by manufacturing process has been considered). With respect to this case, when double feeding is used, the total losses increase between 2.6 dB and 1.5 dB in the 24 GHz ISM band, that is less than the theoretical loss of 3 dB caused by the Wilkinson

dividers on the inner row, excited just at one port (considering the same return loss and coupling conditions). We expect that this improved efficiency is due to the better focus of the energy at the array contour, as already described.

Moreover, as a result of the more concentrated propagation inside the lens, a natural cosine tapering is realized in the lens structure by the application of the double feeding concept. Hence, it can be stated that the overall losses are at least comparable with the case of a typical approach including standard amplitude tapering techniques, but with the advantage of being more compact and directly integrated in the Rotman lens. By the performed analysis, it can be concluded that the proposed feeding concept is wideband in terms of efficiency and reflection coefficients, as shown in Fig. 4.

Finally, we observe that, since all adjacent input ports of the Rotman lens are paired, the phase centers are located at the geometrical mean between single ports centers. For example, referring to Fig. 2, when *Port9* is employed the Wilkinson dividers network excites simultaneously inputs *R9* and *R10*: it is intuitive to see that the relative phase center is located in the middle (corresponding to the focal axes, in this particular case).
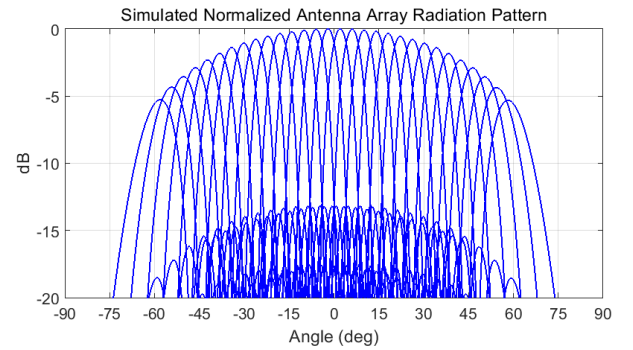
B. Antenna Array

Fig. 5. Simulated normalized antenna array radiation pattern at 24 GHz with ideal excitation, scanning at ±60°.

The radiating elements are an essential part of a radar system, and they qualify the range of coverage and the accuracy of detection. For these reasons, the antenna array should exhibit high directivity, small Half Power Beam Width (HPBW) and low sidelobes levels. It is also preferable to develop the antenna system in a planar structure, for best system integration and easy manufacturing. In this work, a linear array of patch is adopted in combination with the extended scan range Rotman lens system. In order to achieve the required bandwidth, it has been chosen to use a different thickness of substrates for the BFN and the antenna parts. Therefore, as depicted in the central inset of Fig. 2, where the stack-up of the antenna array system is reported, a 508 µm thick Rogers RO4350B substrate has been employed. More in detail, an array of 14 patches for each of the 16 channels has been modeled, as shown in Fig. 2(a). Moreover, it can be noticed from Fig. 2(a) that two parasites columns are inserted on array sides, with the purpose of limiting the effect of the finite dimension of the ground plane. The distance *d* between antenna columns, arranged along the *x* axis, is chosen equal to $\lambda/2$, which allows a 90° based phase shift for enabling the CBS and the BM to be applied (as discussed in Sect. II).

In addition, the double feeding provided by the Wilkinson dividers contributes to lower the sidelobes, imposing an equivalent cosine tapering (see Sect. III-A). The scanning performance of the described array with ideal excitation is shown in Fig. 5, where the maximum scanning is set to ±60° and a scanning loss of 5.3 dB is quantified.

C. Phase Management Unit

The component responsible for the widening of the scan angle is the phase management unit (PMU), placed between the Rotman lens and the array antenna elements. Moreover, the PMU also performs the physical transition from the Rotman lens and the antenna array that are located on different layers, due to design tradeoffs previously discussed.

The PMU is constituted of two parts that perform the CBS and BM separately, as depicted in Fig. 2, where block (b) is accountable for the CBS, and block (c) for the BM. In standard designs, the meandered lines are used to connect the array ports of Rotman lens with the linear antenna array. However, with the proposed concept, there is no need for a well-defined equal phase plane, because the CBS imposes a progressive phase shift. Therefore, the CBS is realized with a set of microstrip lines that introduces the required phase distribution while compensating the length mismatch by adding them together. The complete length of the lines has been split between the two sides of the board for enhancing compactness, leading to an efficient and linear solution as displayed in Fig. 2. This arrangement greatly simplifies the routing, reducing also the PCB area and the conductive losses. In the proposed design, the microstrip to slot-line transition (a well-known technology, widely investigated at millimeter waves, see e.g. [29]), is used as basis for generating the BM operating principle and for coupling signals from the two sides of the board.

As detailed in Sect. II, referring in particular to Fig. 1, the BM is implemented with a proper arrangement of 0° fixed phase shifters (that essentially perform the layer to layer transition) and a 0°/180° reconfigurable phase shifters. However, the implementation of a reconfigurable phase shifter for fulfilling the widening of the scan range concept introduces a necessary selection of the portion of scan range that will be active, while the other would be not operative. The choice of a fast switching device, like PIN diodes, reduces the latency time for changing the state of the BM, and equivalently to switch between the positive and negative scan range angles.
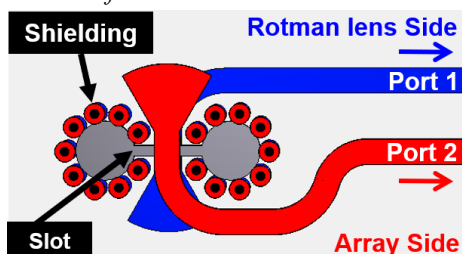
0° Fixed Phase Shifter

Fig. 6. Designed model of the 0° fixed phase shifter (ground planes and dielectric are not shown). The energy is coupled from the Rotman lens side to the array side via the slot. Lines are terminated with a radial stub, while the slot is terminated with an open. The shielding surrounding the slot is also visible.

Fig. 6 shows how the 0° fixed phase shifter has been designed. It is composed of the feeding line located in the Rotman lens side, the output line on the array side and the slot used to couple the energy between the two parts. The two lines and the slot are positioned orthogonally, for ensuring that the electric field is properly coupled. A via fence that follows the contour of the slot prevents the generation of surface waves that would dissipate the energy on the ground planes, including a rise of the crosstalk between adjacent feeding lines. The density of the via fence is imposed by the manufacturing process limits.

Moreover, Fig. 6 displays the use of radial stubs for properly terminating the lines with a virtual short, while an open realized with two circular apertures is employed for terminating the slot [30]. Finally, as mentioned in Sect. III, the microstrip lines on the two layers have the same width but different characteristic impedance (50 Ω for the Rotman lens side, while the array side has 75 Ω) given by the different choice of substrate; in this way a compact and symmetric design of the microstrip-slot interface is obtained. In fact, a wider line on array side would have required a longer slot (placed perpendicularly to the line) and a larger bending for routing the phase shifter connection to the antenna column.

0°/180° Reconfigurable Phase Shifter
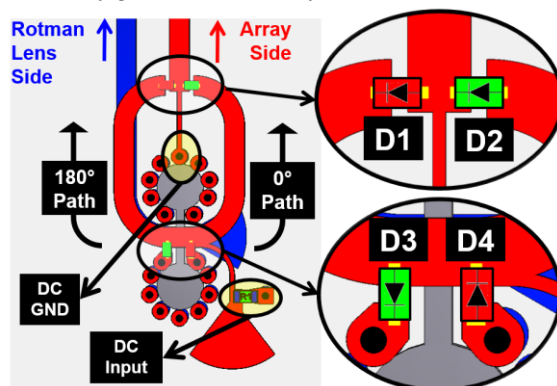

Fig. 7. Complete model of the 0°/180° reconfigurable phase shifter, constituted by 4 PIN diodes; 0° configuration (shown in this example): *D2* and *D3* are ON, *D1* and *D4* are OFF; instead, for obtaining the 180° case, *D1* and *D4* are ON, and *D2* and *D3* OFF.

In Fig. 7, the structure of the 0°/180° reconfigurable phase shifter is reported, which shares the same layer to layer transition described in the previous paragraph, but it includes four PIN diodes in the array side, devoted to produce either the two phase shifting conditions. It is also noticed that the microwave active part has been placed on array side, in such a way that no in-line decoupling capacitors are needed. The phase shifting takes advantage of the slot-microstrip coupling, that can be considered as a splitter, whose outputs are 180° degree out of phase. The phase selection is achieved by properly biasing the four PIN diodes, used for enabling one of the two branches (*0° path* or *180° path*) positioned at sides of the slot, for coupling the electric field with the desired polarity.

More specifically, referring to Fig. 7, diodes *D1* and *D2* are placed in series, while *D3* and *D4* are connected to ground, on the two sides of the slot, as closest as possible, for terminating the microstrip-to-slot transition. The configuration for

achieving 0° phase shifting is obtained by direct biasing *D2* and *D3* (the *0° path* is active), while *D1* and *D4* are reverse biased. It can be noticed that this configuration is equivalent to the 0° fixed phase shifter (see Fig. 6), with the difference that, in this case, the virtual short is fulfilled by setting the diode *D3* ON. In the dual case, in which the diodes *D1* and *D4* are active while *D2* and *D3* are OFF, the *180° path* is selected, and the phase inversion is achieved. It is remarked that in principle only two diodes can be used for achieving the same functionality, however this approach results in inadequate performance due to limited isolation in the OFF state of the PIN diodes at 24 GHz.

In Fig. 7, the structures developed for the correct biasing of the diodes (i.e. *DC input* and *DC GND*) are also indicated, and they have been specifically tuned for avoiding mismatch/losses on the 0°/180° reconfigurable phase shifter. In particular, the positive/negative current is injected at *DC input*, where a *λ/4* line terminated on a radial stub is used as connection with a resistor, while the *DC GND* point is used as ground reference by exploiting a *λ/4* line connected directly to ground.

For the required biasing of the pairs of series-shunt diodes (*D1* and *D4* or *D2* and *D3*), a positive/negative voltage is used as control, namely $V_{pos}= 5$ V and $V_{neg}= -5$ V. Specifically, with V_{pos} the diodes *D2*, *D3* are ON and positive angles of the scanning range are selected, while V_{neg} sets to ON the diodes *D1* and *D4* for scanning the negative range. In particular, the MACOM MA4FCP200 PIN diode [31] has been chosen, due to low parasitic elements and low series resistance at the frequency range of interest. Finally, we underline that is essential, for a correct design, to use, in the full-wave simulations, a detailed model of the PIN diodes. Hence, for proper modelling the diode, an equivalent lumped circuit has been extrapolated from S-parameters: the values used in the ON state of the diode were $R_{ON} = 6.5\ \Omega$ and $L_{ON} = 0.15$ nH, while for the OFF configuration the equivalent capacitance $C_{OFF} = 25$ fF was applied. These parameters were then included in a detailed 3-D model of the component, for enhancing accuracy.

IV. NUMERICAL AND EXPERIMENTAL VALIDATION

The extended scan range method applied to the Rotman lens as beamformer has been validated by fabricating and testing the complete described system, already reported in Fig. 2. According to Fig. 2, the overall dimensions of the PCB are L=130 mm and H=140 mm. Being manufacturing and cost issues a goal of this research activity, a standard fabrication process has been used. Therefore, for a more reliable soldering process of the components, especially for the tiny dimensions (380 μm x 230 μm) of PIN diodes, a standard Electroless Nickel Immersion Gold (ENIG) has been adopted as copper finishing. Moreover, by considering the high number of inputs, the SMP connectors have been selected as a low-cost alternative to the 2.92 mm connectors, being suitable for high density surface mount interconnections and, then, for the reduction of the form factor of the PCB. In fact, SMP connectors have the advantage of being compact, requiring very little space for positioning adjacent connections (thanks to their snap-on coupling). This feature allows to arrange the input lines in a radial pattern, as shown in Fig. 2, keeping an almost constant length.

Nevertheless, cares must be taken when performing measurements with SMP, due to the mechanically fickle connection, as detailed in the following.

The overall performance of the extended scan range array based on Rotman lens and the phase shifters have been evaluated through conductive measurements. Furthermore, the radiation pattern of the complete scanning array system has been tested in the anechoic chamber. For both characterizations a 2.92 mm to SMP adapter has been introduced for interfacing the device under test with the Vector Network Analyzer (VNA). Moreover, 50 Ω SMP terminations have been plugged on all the unused ports in both S-parameters and radiation measurements. In Fig. 8(a) the test setup used for the measurements of the scattering matrix is shown, while in Fig. 8(b) the picture for the far field measurement setup is presented. During measurements, the BM operative state is selected by acting on a sliding switch, connected at the outputs of a dual linear dropout regulator able to provide V_{pos} and V_{neg} (i.e. ±5 V, thanks to a regulated charge pump configuration), located on Rotman lens side (visible in Fig. 2 on bottom right corner). This easy way of controlling the BM greatly simplifies the measurement process: for instance, the measurement of the radiation pattern associated with one input can be performed in both states by simply positioning the switch for selecting the positive/negative voltage (i.e. positive/negative scan angles).
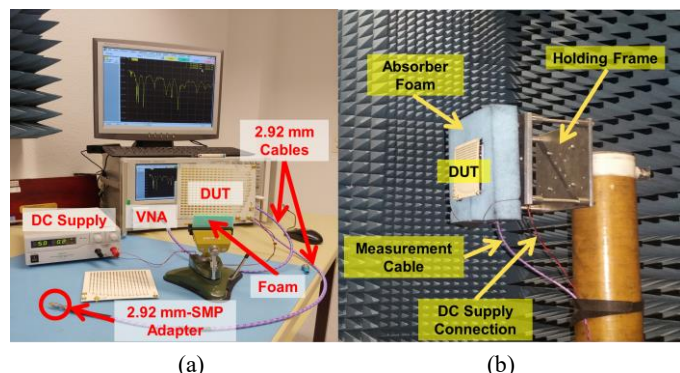

(a)   (b)

Fig. 8.   Measurement test setups: in *(a)* the Vector Network Analyzer is employed for measurement of S-parameters, while in *(b)* the antenna pattern measurement setup in the anechoic chamber is shown. Main components of the two test benches are indicated.

A. Phase Shifters

The designed phase shifters have been realized and tested by mean of a separate test structure, since they are the most challenging part of the overall system. Fig. 9 shows the measured phase shifters (see Sect. III-C); specifically, in Fig. 9(a), the array side part of the fixed phase shifter is displayed, while in Fig. 9(b) the reconfigurable phase shifter is shown. Finally, Fig. 9(c) reports the phase shifter part etched on Rotman lens side, which is common for both designs.

Unfortunately, for measuring such devices, the TRL method cannot be used, since the input and output ports have different characteristic impedances (i.e. dissimilar substrate thickness and consequently different tuning of the SMP-microstrip transition), as discussed in Sect III-C. Moreover, also the time gating can not be used, because the resolution for differentiating the effects of the connector and the phase shifters was insufficient, due to the small physical size of the structure.
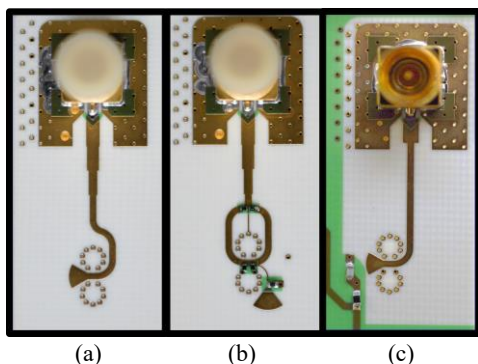
Fig. 9. Manufactured and measured phase shifters, including the SMP connector; *(a)* 0° fixed phase shifter, array side; *(b)* 0°/180° reconfigurable phase shifter, array side; *(c)* 0° fixed and 0°/180° reconfigurable phase shifter, Rotman lens side (identical for the two types of phase shifters).

For characterization purposes, a three stages quarter wavelength impedance transformer was added on the array side part of both phase shifters (as can be recognized in Fig. 9(a) and Fig. 9(b)), for performing the 75 Ω to 50 Ω transition and establishing a proper connection with the VNA. Hence, the two phase shifters are first characterized through numerical simulations, without the presence of the SMP connectors and the three stages impedance transformer (see Fig. 6 and Fig. 7), for distinctly evaluating their performance in the BM process. Then, the validity of the obtained measured results is indirectly proven by embedding the model of the connector and the three stages impedance transformer in the simulation, in order to have the same configuration, as in Fig. 9. By this procedure, a clearer and reliable comparison between the simulated and measured results are possible.
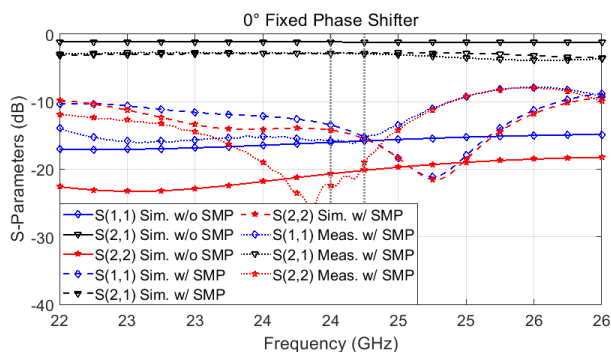

Fig. 10. Simulated S-parameters of the 0° fixed phase shifter without the SMP connector (solid lines) and comparison between simulation and measurements including the connector (respectively dashed and dotted lines); 24 GHz ISM band highlighted for reference.

Therefore, Fig. 10 displays the reflection coefficients of the 0° fixed phase shifter in the frequency band 22 GHz to 26 GHz in the cases with SMP connectors included (through simulation and measurements) and without (only simulated results). The latter case takes into consideration the ideal situation where the connector and the three stages impedance transformer are not integrated. It is reminded that the S-parameters reported in this case are calculated considering a characteristic impedance of 50 Ω for the input at Rotman lens side and 75 Ω for the one placed on array side. The analysis of the S-parameter of the fixed phase shifter reveals a good performance in the frequency range of interest, where the introduced losses are less than 1.3 dB.

Similar performance can be observed also in the wider frequency range, shown in Fig. 10. It can be noticed that the resistive losses are quite high mainly because the actual conductivity of the ENIG finishing, which is much lower compared to solid copper, has been considered in the simulations. The conductivity of the ENIG is very sensitive to the manufacturing process, and, then, its value, inserted in the simulation ($\sigma = 5.6 \cdot 10^6 \, S/m$ in the range $22 - 26$ GHz), was extrapolated by measurements. In the second case, where SMP connectors and the three stages impedance transformer are both included, a direct comparison between simulated and measured results can be performed. Clearly, the introduction of these components causes a degradation of the overall performance, as noticed in both measured and calculated values of the scattering parameters reported in Fig. 10. Nevertheless, a good agreement between the two results is recognized, where the shift to lower frequency of the $|S_{11}|$ and $|S_{22}|$ can be explained by the presence of the 2.92 mm to SMP adapter used during the measurement process that was not included in the VNA calibration.
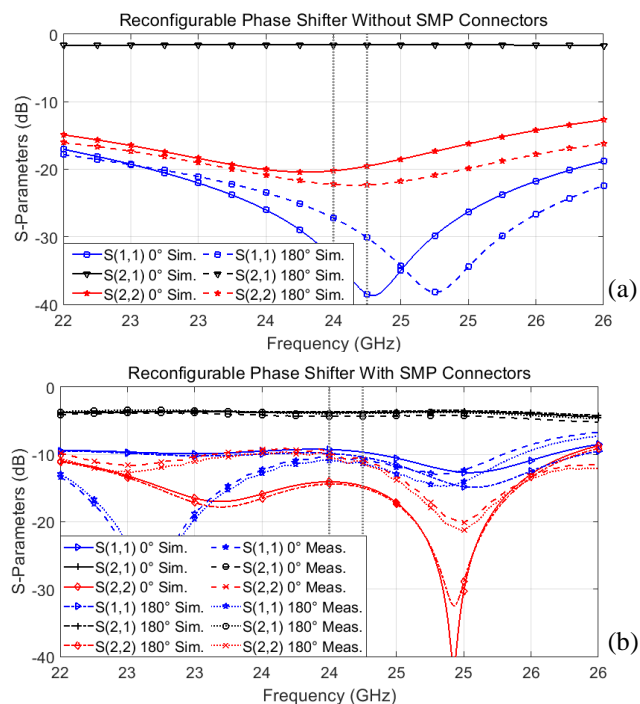

Fig. 11. Scattering parameters of the 0°/180° reconfigurable phase shifter in both BM states; *(a)* simulated *without* the SMP connector; *(b)* measured and simulated including the SMP connector; 24 GHz ISM band highlighted.

Then, in Fig. 11, the reconfigurable phase shifter is analyzed. It can be noticed that, from the numerical results displayed in Fig. 11(a), losses increased slightly compared to the one calculated in Fig. 10 in the analogous case without connectors and impedance transformer: 1.9 dB for the reconfigurable phase shifter versus 1.3 dB for the fixed version in the 24 GHz ISM band, where the same port termination scheme was adopted. The slightly higher losses are due to the parasitic elements of PIN diodes, in both ON and OFF states (see Sect III-C). Moreover, it is recognized that $|S_{11}|$ and $|S_{22}|$ are not identical: this is due to the microwave DC decoupling which loads in a different way the active branches of the phase inverter, thus breaking its symmetry. For the same reason, the

reflection coefficients $|S_{ii}|$ present a shift in frequency in the case of 0° (BM not active) with respect to the case of 180° shift (BM activated). The results reported in Fig. 11(b) show some small discrepancies between the simulated and measured amplitude of the reflection coefficients $|S_{11}|$ and $|S_{22}|$. This can be explained with a not perfect equivalent electric modelling of the PIN diodes, in particular the values of C_{OFF} and L_{ON} reported in Sect III-C. These two equivalent electrical components are affecting mostly the reflection coefficients, rather than the losses that are typically driven by the resistive part of the model (denoted as R_{ON}), which instead show a good agreement between the two displayed curves of $|S_{12}|$.
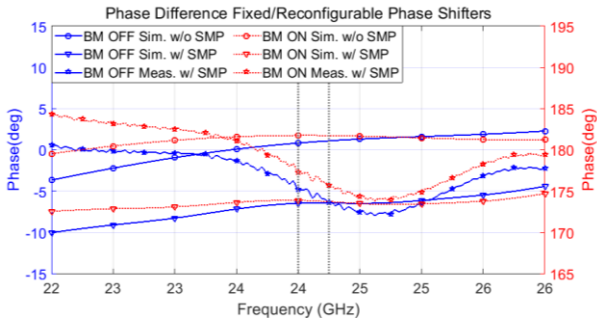

Fig. 12. Differential phase between the reference (0° fixed phase shifter) and the 0°/180° reconfigurable phase shifter in the case BM OFF (solid lines, left *y* axis) and BM ON (dotted lines, right *y* axis); 24 GHz ISM highlighted.

In analogy with the evaluation carried for the magnitude of the S-parameters, the phase is analyzed. In particular, Fig. 12 displays the differential phase relative to the S_{12} parameter between the fixed phase shifter and the reconfigurable phase shifter in the BM inactive state (i.e. 0° phase is added to the line), and the BM active state (i.e. 180° phase inversion superimposed to the phase distribution). Referring to the simulated results of the model without the SMP connectors, we can observe that in the 24 GHz ISM band the phase error is very limited in both BM operative states, and the designed system has potentially more than 6 GHz bandwidth following the ±5° error criterion (from 21.55 GHz to 27.65 GHz). Instead, in the cases where the SMP connectors are included, the measured phase difference is consistent with the corresponding simulated results in both BM states, even if the measured ones are affected by some fluctuation, probably derived from the fickle mechanical contact. According to Table I, which summarizes the phase errors in the examined cases, a measured maximum deviation from the theoretical values of 6.4° in the 24 GHz operative band is recognized. Moreover, the comparison with the case without SMP confirms that the transition microstrip-connector introduces a discontinuity that causes a mismatch.

TABLE I
MAXIMUM DIFFERENTIAL PHASE ERROR

	Sim. w/o SMP		Sim. w/ SMP		Meas. w/ SMP	
BM Status	**0°**	**180°**	**0°**	**180°**	**0°**	**180°**
24 – 24.25 GHz	0.9°	1.7°	6.4°	6.3°	6.4°	4.2°
22 – 26 GHz	3.6°	1.8°	10°	7.4°	7.9°	5.9°

Similarly to the analysis carried for the magnitude of the scattering parameters, also in this case the discrepancies found in the simulated and measured phase errors can be explained with inaccuracies in the equivalent electrical model of the PIN

diode. Finally, by considering the good agreement of the simulated and measured results including SMP, it can be assumed that the performance of the phase shifters is reasonably close to the one displayed in the simulations without connectors.

B. Complete System

In Fig. 13, input reflection coefficients of the complete system, shown in Fig. 2, are evaluated by means of simulations and measurements. In this structure, the effect of the SMP connector to microstrip transition can be excluded from the measurements by applying the time gating technique. In fact, in this case the reflections at connector interface are clearly discriminated from the others relative to the Wilkinson dividers due to the long input lines, and they can be eliminated accordingly. Specifically, only S-parameters relative to the case of BM not activated (i.e. for positive bias voltage of PIN diodes) are displayed in Fig. 13, because the other case is analogous. For a better analysis the wider frequency band of 20 – 30 GHz is considered, and the 24 GHz ISM band is shown for reference.
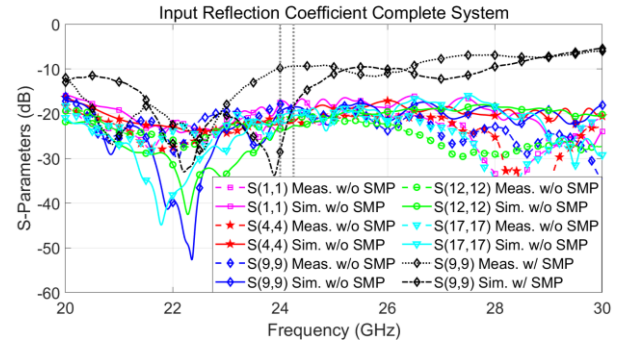

Fig. 13. Simulation (continuous line) and time gating measurements (dashed lines) of the reflection coefficients for ports 1, 4, 9, 12 and 17 relative to the complete system *without* SMP connectors and BM not activated. Simulated and measured results in the case *with* SMP connectors (dash-dotted and dotted lines respectively) are reported for *Port9*; 24 GHz ISM band is highlighted.

The results in Fig. 13 exhibit a variability of the reflection coefficient across the input ports, mostly due to the asymmetry of the system (given by the CBS and the BM arrangements). However, the predicted reflection coefficient is found to be consistent with the performed measurements with time gating, even if the simulated values in *Port9, Port12* and *Port17* denote a better matching level at lower frequencies (with minimum at 22 GHz) with respect to measurements. By considering as reference the central port in Fig. 13 (i.e. *Port9* indicated with the diamond marker), in both cases where the SMP connectors are included or removed by applying the time gating technique, a good agreement between measured and corresponding numerical results is observed.

In particular, the curves relative to simulations and measurements with connectors clearly show the degradation due to the SMP to microstrip transition, in comparison with the equivalent cases without connector. The shift in frequency between the ungated measurement and the simulated S-parameters can be explained by the SMP to 2.92 mm adapter used during measurements, and not included in the simulation. Nevertheless, it can be stated that even with SMP connectors, the extended scan range phased array is well matched in the 24 GHz ISM band (minimum measured value is 9.85 dB).
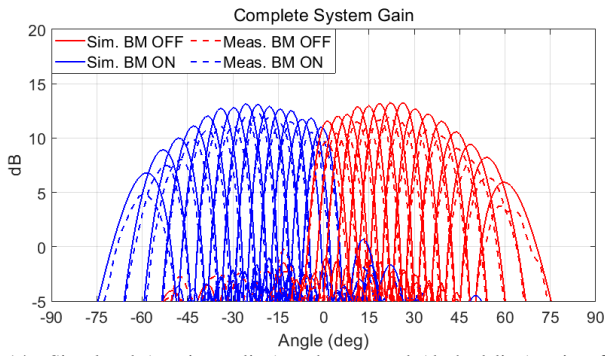
Fig. 14. Simulated (continuos line) and measured (dashed line) gain of the realized extended scan range array at 24GHz; different colours are used to distinguish between the case of BM activated (negative scanning angles) and BM not activated (positive scanning angles).

Fig. 14 shows the simulated and measured gain pattern at 24 GHz in the *xz* plane (refer to Fig. 2 for axes definition). Considering the overall scanning range, it is noticed that the results obtained by measurements are in good agreement with the simulated ones, confirming that the described method is actually able to almost double the FOV of a scanning array using a Rotman lens as beamformer. In fact, the maximum FOV is detected at 58.7°, which is close to the theoretical value of 60°. The difference of 1.3° can be produced by the many factors, and they are mainly due to tolerances in the fabrication of the prototype.

For a clearer overview of the performance of the extended scan range antenna system, the main parameters displayed in Fig. 14 are summarized in Table II, where the measured realized gain and HPBW are reported for each beam (associated with a scanning angle). The two measured quantities are also compared with the results obtained by simulation. The difference between the simulated and measured gain pattern, quantified to be between 0.7 dB and 2.2 dB, is explained by considering the losses of the SMP connectors (estimated to be about 0.7 dB at 24 GHz), inaccuracies in the modeling of components (e.g. PIN diodes) and the conductivity of the ENIG finishing. It is interesting to notice that the maximum values of the gain are not located at broadside; instead, they are located at angles in proximity of ±30° (corresponding to the initial maximum FOV of the Rotman lens). This can be explained by considering that the central input ports realize a more efficient illumination of the array contour of the Rotman lens, compare to ports placed on the sides, where a larger amount of power is coupled to the dummy ports due to the geometry of the lens (see

Sect. III-A). However, the peak of the gain is not associated with the beam positioned at ±30°: this is because of the scan loss at these angles (numerically estimated to be 1 dB). In fact, this characteristic shape of the gain pattern having the highest values at approximately ±25° and reducing at lower and higher angles is the sum of two different effects: the scan loss and the illumination loss. The illumination loss concerns both the beams positioned at widest and lowest scan angles, and its effect has been estimated to be 1.2 dB, by comparing the level of beam at broadside (scan loss at low scan angles is negligible) with respect to the beam at ±30° that represent the cases with best illumination of the lens (scan loss associated with this angle is considered in the calculation). Moreover, at extreme angles of the scanning range, illumination loss causes the same amount of gain reduction discussed for the broadside case, but at increasing scan angles the effects of the scan loss became dominant, as recognized in Fig. 5, where the reduction was estimated to be 5.3 dB at ±60°. Furthermore, from both measured and simulated antenna gains reported in Table II, an asymmetry of the levels of the beams is recognized for opposite angles of the scan range. This difference can be explained by the overall insertion loss among each column of antenna array, caused by the CBS structure (i.e. longer lines used for generating the required phase distribution are intrinsically asymmetric), and by the amplitude mismatch that appears at each column due to the alternation of fixed and reconfigurable phase shifters (the last are more lossy, because of the presence of PIN diodes). This fact also explains the slightly uneven levels of some adjacent beams (e.g. beam at 11.3° compared to beam at 15°), as can be recognized from the values reported in Table II. Nevertheless, it can be noticed that the performance of the designed prototype exhibits a reduction of the realized gain of maximum 3 dB, in the scanning range ±45°. In addition, it can be also observed that the spatial coverage of the beams is ensured by their tight overlapping, as a result of the BM application. In fact, not only the scan range is doubled, but also the number of available beams, which introduce the possibility to use a Rotman lens with half of beam ports with respect to standard designs.

Finally, Fig. 15 shows the normalized amplitude of the co- and cross- components of the radiated field relative to *Port11* (as indicated in Fig. 2(e) enclosure), proving that the measured radiation patterns are correctly predicted by the numerical modelling. This result verifies also that the analysis carried in Sect. IV-A on phase shifters performance is consistent, and it confirms the accurate phase distribution obtained by simulation for the models without SMP connectors.

TABLE II
COMPARISON AMONG SIMULATED AND MEASURED GAIN AND HALF POWER BEAMWIDTH OF THE ROTMAN LENS BASED SCANNING ARRAY

| Scan Angles	-58.7°	-52.8°	-47.8°	-42.9°	-38.4°	-33.7°	-29.5°	-25.5°	-21.5°	-17.6°	-14.0°	-10.5°	-7.2°	-4.1°	-0.8°
Gain Sim.(dB)	6.8	8.9	10.0	11.1	12.0	12.7	12.8	13.1	13.0	12.8	12.7	12.5	11.7	11.8	11.0
Gain Meas.(dB)	4.8	7.5	8	9.9	10.7	11.1	11.1	11.9	12.3	11.9	11.3	10.5	10.3	10.5	9.9
HPBW Sim.	12.9°	10.9°	9.9°	9.1°	8.5°	8.0°	7.7°	7.4°	7.1°	7.0°	7.0°	6.8°	7.1°	7.1°	6.9°
HPBW Meas.	13.4°	10.7°	10.0°	8.9°	8.6°	7.6°	7.2°	7.2°	6.7°	7°	7.2°	6.8°	7.3°	6.8°	6.8°
Scan Angles	1.3°	4.8°	8.0°	11.3°	15.0°	18.6°	22.2°	26.3°	30.4°	34.3°	39.2°	43.8°	48.6°	54.0°	59.6°
Gain Sim.(dB)	11.5	12.0	12.2	12.8	12.9	13.1	13.2	13.2	12.6	12.2	11.5	10.5	9.4	8.2	5.9
Gain Meas.(dB)	9.7	10.4	10.3	11.5	11.0	11.6	12.0	11.4	10.8	10.7	10.2	9.0	7.9	6.3	3.7
HPBW Sim.	7.0°	7.0°	7.1°	6.9°	6.9°	7.2°	7.3°	7.4°	7.7°	8.0°	8.5°	9.2°	10.0°	11.0°	13.1°
HPBW Meas.	7.1°	7.0°	7.2°	6.8°	7.0°	7.3°	7.1°	7.3°	7.8°	7.9°	8.4°	9.5°	10.0°	11.4°	13.3°
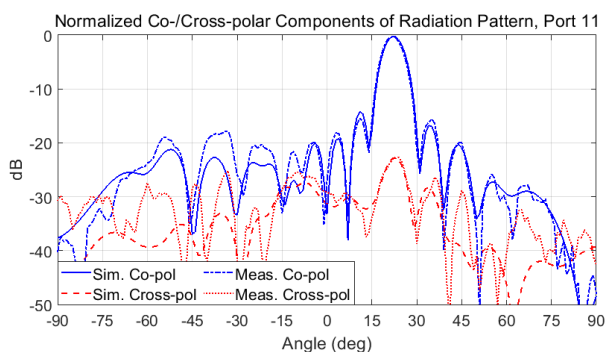
Fig. 15. Comparison of the normalized co-polar and cross-polar components of the radiation pattern for *Port11* at 24 GHz obtained through simulation and measurement in case of BM OFF.

This aspect is particularly important for radar applications, and it is considered a parameter that qualifies the designed phased array. In addition, it is observed that the level of sidelobes is below 10 dB in any condition (worst case), without any additional amplitude tapering at antenna inputs, thanks to the proposed double feeding structure of the Rotman lens (see Sect. III-A). Furthermore, it is noticed that the double feeding concept allows to further decrease the level of sidelobes by combining more inputs to be simultaneously excited: this is possible by adding an additional level of Wilkinson dividers (e.g. three stages of Wilkinson dividers instead of two as developed in this work). Table III provides a comparison among wide scan angles designs of phased arrays based on Rotman lens as beamformer available in literature, where [22] and [23] are considered in particular, as previous examples of widening scan range researches.

Finally, the cross-polar component of the radiation pattern is found to be lower than -15 dB respect to the measured co-polar field pattern, as shown for *Port11* in Fig. 15.

TABLE III
COMPARISON AMONG ROTMAN LENS BASED SCANNING ARRAYS

Ref.	Freq.	Technology	Scan Range	Scan Extension	SLL
[22]	24 GHz	PET	±38°	8°	10 dB
[23]	9 GHz	LC phase shifters	±37.5°	7.5°	12 dB*
[16]	24 GHz	SIW	±48°	–	10 dB*
[18]	60 GHz	LTCC	±30°	–	12 dB
[19]	10 GHz	Synthesized dielectric	±33°	–	10 dB
This work	24 GHz	PIN diodes	±60°	30°	10 dB

(*) Estimated graphically

V. CONCLUSION AND PERSPECTIVES

In this paper, an innovative method for extending the scanning range of a phased array based on the concepts of Complete Beam Shifting and Beam Mirroring has been presented. The proposed technique has been demonstrated and validated in combination with a Rotman lens, by employing both numerical tools and measurements. As a result, by considering an initial 24 GHz trifocal Rotman lens able to achieve a FOV of ±30°, a compact and cost-effective design of a 24 GHz ISM scanning array radar was implemented, demonstrating a doubled maximum steering angle of about ±60°.

Moreover, for achieving the BM, a proper reconfigurable phase shifter has been developed and realized, showing good performance and simple control requirements. The overall performance of the phased array based on Rotman lens as beamformer has been enhanced by a novel multiple feeding concept, that improves the illumination of the antenna side contour of the lens, thus decreasing the losses due to spillover and generating a cosine tapering. Finally, the purpose of building a low-cost product has driven the design to use solutions (e.g. use of SMP connectors and ENIG copper finishing) that have caused a decrease in the system efficiency. Hence, to overcome the limitations of the current design, an improvement on the manufacturing (i.e. connectors and surface finishing) will be considered.

As a more sophisticated development of this concept, the PMU could introduce the flexibility to switch between the normal Rotman lens operation (i.e. no alteration to the Rotman lens progressive phase shifting) and the extended scan range modus. The normal Rotman Lens operation would be useful for accomplishing tasks when the highest gain must be at broadside, for scanning with highest performance at small scan angles. Instead, when a wider scan range is required, the CBS and BM would be activated.

As further perspective, this concept will be transferred to a radar system for 77 GHz operation that will necessarily require new definitions of the phase management unit and antenna array.

REFERENCES

[1] C. Y. Chang, "*Advancements, prospects, and impacts of automated driving systems,*" International Journal of Transportation Science and Technology, Vol: 6, no. 3, pp: 208-216, 2017.

[2] W. Rotman and R. F. Turner, "Wide-angle microwave lens for line source applications," *IEEE Trans. Antennas Propag.*, vol. AP-11, pp. 623–632, 1963.

[3] R. C. Hansen, "Design trades for Rotman lenses", IEEE Trans. Antennas Propag., vol. 39, no. 4, pp. 464-472, April 1991.

[4] J. P. Shelton, "Focusing characteristics of symmetrically configured bootlace lenses," IEEE Transactions on Antennas and Propagation, vol. 26, no. 4, pp. 513–518, 1978.W.-K. Chen, *Linear Networks and Systems*. Belmont, CA: Wadsworth, 1993, pp. 123–135.

[5] T. Katagi, S. Mano, and S. Sato, "An improved design method of Rotman lens antennas," *IEEE Transactions on Antennas and Propagation*, vol. 32, no. 5, pp. 524–527, 1984.

[6] D. R. Gagnon, "Procedure for correct refocusing of the Rotman lens according to Snell's law," *IEEE Transactions on Antennas and Propagation*, vol. 37, no. 3, pp. 390–392, 1989.E. P. Wigner, "Theory of traveling-wave optical laser," *Phys. Rev.*, vol. 134, pp. A635–A646, Dec. 1965.

[7] P. Simon, "Analysis and synthesis of Rotman lenses," in Proc. of the 22nd AIAA International Communications Satellite Systems Conference & Exhibit, Monterey, CA, USA, May 2004.

[8] E. O. Rausch and A. F. Peterson, "Rotman lens design issues," in Proceedings of the IEEE Antennas and Propagation Society International Symposium and USNC/URSI Meeting, vol. 2, pp. 35–38, July 2005.

[9] N.J.G Fonseca, "A Focal Curve Design Method for Rotman Lenses With Wider Angular Scanning Range," IEEE Antennas. And Wireless Propag. Letters, vol. 16, pp. 57-59, Apr. 2016.

[10] L. Ferreira Filho, M.M. Mosso, "A New Concept of Microstrip Rotman Lens Design", in Proc. of 2015 IEEE MTT-S Int. Microwave and Optoelectronics Conference, Porto de Galinhas, Brazil, 3-6 Nov. 2015.

[11] P. K. Singhal, P. C. Sharma and R. D. Gupta, "Design and analysis of Rotman type lens using hyperbolic focal arc for wide angle scanning," 1999 Asia Pacific Microwave Conference. APMC'99. Microwaves Enter the 21st Century. Conference Proceedings (Cat. No.99TH8473), Singapore, 1999, pp. 932-935 vol.3.

[12] P. K. Singhal, P.C. Sharma, and R. D. Gupta, "Rotman lens with equal height of array and feed contours", IEEE Trans. on Antennas and Propag., vol. 51, Issue 8, pp. 2048-2056, Aug. 2003.

[13] J. Dong, A. I. Zaghloul, and R. Rotman, "Non-focal minimum phase-error planar Rotman lens," in Proceedings of the URSI National Radio Science Meeting, Boulder, CL, USA, 2008.

[14] M. Rajabalian and B. Zakeri, "Optimisation and implementation for a non-focal Rotman lens design," in *IET Microwaves, Antennas & Propagation*, vol. 9, no. 9, pp. 982-987, 18 6 2015.

[15] E. Sbarra, L. Marcaccioli, R. V. Gatti and R. Sorrentino, "A novel rotman lens in SIW technology," 2007 European Radar Conference, Munich, 2007, pp. 236-239.

[16] K. Tekkouk, M. Ettorre and R. Sauleau, "SIW Rotman Lens Antenna with Ridged Delay Lines and Reduced Footprint," in *IEEE Trans. on Microwave Theory and Tech.*, vol. 66, no. 6, pp. 3136-3144, June 2018.

[17] J. Pourahmadazar and T. A. Denidni, "Multi-beam tapered slot antenna array using substrate integrated waveguide Rotman lens," *2015 European Radar Conference (EuRAD)*, Paris, 2015, pp. 425-428.

[18] A. Attaran, R. Rashidzadeh and A. Kouki, "60 GHz Low Phase Error Rotman Lens Combined With Wideband Microstrip Antenna Array Using LTCC Technology," in *IEEE Transactions on Antennas and Propagation*, vol. 64, no. 12, pp. 5172-5180, Dec. 2016.

[19] L. Schulwitz and A. Mortazawi, "A New Low Loss Rotman Lens Design for Multibeam Phased Arrays," 2006 IEEE MTT-S International Microwave Symposium Digest, San Francisco, CA, 2006, pp. 445-448.

[20] T. K. Vo Dai, T. Nguyen and O. Kilic, "Compact multi-layer microstrip Rotman lens design using coupling slots to support millimetre wave devices," in *IET Microwaves, Antennas & Propagation*, vol. 12, no. 8, pp. 1260-1265, 4 7 2018.

[21] F. C. Suárez, D. N. Méndez and M. Baquero-Escudero, "Rotman lens with Ridge Gap Waveguide technology for millimeter wave applications," *2013 7th European Conference on Antennas and Propagation (EuCAP)*, Gothenburg, 2013, pp. 4006-4009.

[22] Sang-Gyu Kim, P. Zepeda and Kai Chang, "Piezoelectric transducer controlled multiple beam phased array using microstrip Rotman lens," in IEEE Microwave and Wireless Components Letters, vol. 15, no. 4, pp. 247-249, April 2005.

[23] S. Christie, R. Cahill, N. Mitchell, Y. Munro and A. Manabe, "Electronically scanned Rotman lens antenna with liquid crystal phase shifters," in Electronics Letters, vol. 49, no. 7, pp. 445-447, Mar. 28 2013.

[24] A. Lauer, O. Litschke, "Kompakte Richtantennenanordnung mit Mehrfachnutzung von Strahlerelementen," Deutsches Patent- und Markenanmt DE10 2007 055 534 B4, 09 Aug., 2018.

[25] E. Tolin, O. Litschke, S. Bruni and F. Vipiana, "Innovative Rotman lens setup for extended scan range array antennas," 2017 IEEE-APS Topical Conference on Antennas and Propagation in Wireless Communications (APWC), Verona, Italy, 2017, pp. 252-255

[26] E. Tolin, O. Litschke and F. Vipiana, "Phase management for extended scan range antenna arrays based on Rotman lens," 2018 12th European Conference on Antennas and Propagation (EUCAP), London, 2018.

[27] E. Tolin, O. Litschke, S. Bruni and F. Vipiana, "Phase shifters design for Rotman lens based beamforming network scan range extension, "2018 IEEE International Symposium on Antennas and Propagation and USNC-URSI Radio Science Meeting, Boston, 2018.

[28] EMPIRE XPU Manual - Version 7.70, IMST GmbH, Kamp Lintfort, Germany, 12 December 2017.

[29] K. C. Gupta R. Garg I. Bahl P. Bhartia Microstrip Lines and Slotlines MA Noorwood:Artech House 1996

[30] B. Shuppert, "Microstrip/slotline transitions: modeling and experimental investigation," in IEEE Transactions on Microwave Theory and Techniques, vol. 36, no. 8, pp. 1272-1282, Aug. 1988.

[31] MACOM, "Flip chip PIN diode," MA4FCP200 datasheet, Rev. V5.

Enrico Tolin received the M.Sc. degree in electronic engineering from Università degli Studi di Padova, Italy, in 2008. From 2010 to 2014, he worked as a R&D engineer at Calearo Antenne SPA, Vicenza, Italy. Since 2014, he is part of the Antennas & EM Modelling group at IMST GmbH, Germany. Currently, he is a PhD Student at the Dept. Electronical and Telecomunication Engineering, Politecnico di Torino, Torino, Italy. His research interests include the design of reconfigurable antennas and systems, integrated antennas, antenna arrays, active and passive circuits and low noise amplifiers.

Oliver Litschke received the M.Sc. degree in Electrical Engineering from Duisburg-Essen University, Germany, in 2001. Since 2001 he is working at IMST GmbH as R&D senior engineer and project manager, acquiring and working in several funded and industrial projects for satellite and mobile communications, as well as radar applications. Since 2009 he leads the Antenna Front-ends group at IMST GmbH. His current main research interests include the design of high-frequency antennas arrays, high integration technologies for compact antenna arrays, measurement techniques for antenna systems and passive filter design.

Simona Bruni received the laurea degree in telecommunication engineering and the Ph.D. degree in electromagnetics from the University of Siena, Italy, in 2002 and 2006 respectively. Her Ph.D. was financed and hosted by the Defence, Security and Safety Institute of the Netherlands Organization for Applied Scientific Research (TNO), The Hague, where afterwards she worked as antenna researcher for one year. From 2007 to 2013, she worked as an R&D antenna engineer at Calearo Advanced Techonogy (CAT) department, in Calearo SPA, Vicenza, Italy. Since 2013, she has joined the Antennas & EM Modelling group at IMST, GmbH where she work as R&D antenna engineer in the Antenna Front-ends team. Her research interests include the design of integrated antennas, high-frequency antenna arrays and front-end design for communications and automotive applications.

Francesca Vipiana (M'07–SM'13) received the Laurea and Ph.D. degrees in electronic engineering from the Politecnico di Torino, Torino, Italy, in 2000 and 2004, respectively. Her doctoral research was carried out partly at the European Space Research Technology Center, Noordwijk, The Netherlands. From 2005 to 2008, she was a Research Fellow with the Department of Electronics, Politecnico di Torino. From 2009 to 2012, she was the Head of the Antenna and EMC Laboratory, Istituto Superiore Mario Boella (ISMB), Torino. Since 2012, she has been an Assistant Professor with the Department of Electronics and Telecommunications, Politecnico di Torino, where she has been an Associate Professor since 2014. She is involved in the analysis, synthesis, and optimization of multiband reconfigurable compact antennas, and the modeling and design of microwave imaging systems for medical applications. Her current research interests include numerical techniques based on the integral equation and method of moment approaches, with a focus on multiresolution schemes, domain decomposition, preconditioning and fast solution methods, and advanced quadrature integration schemes.

Prof. Vipiana received the Young Scientist Award from the Union of Radio Science General Assembly in 2005, the First Prize in the poster competition from the First IEEEWomen in Electromagnetics Workshop in 2009, the ISMB Best Paper Award in 2011, and the Lot Shafai Mid-Career Distinguished Award from the IEEE Antennas and Propagation Society in 2017. She is currently in the Editorial Board of the IEEE Transactions on Antennas and Propagation and of the IEEE Antennas and Propagation Magazine.